Journal of Biomedical Optics

BiomedicalOptics.SPIEDigitalLibrary.org

Photoacoustic and ultrasound imaging of cancellous bone tissue

Lifeng Yang
Bahman Lashkari
Joel W. Y. Tan
Andreas Mandelis

SPIE.

Photoacoustic and ultrasound imaging of cancellous bone tissue

Lifeng Yang,[a,b] Bahman Lashkari,[b,*] Joel W. Y. Tan,[b] and Andreas Mandelis[a,b]
[a]University of Electronic Science and Technology of China, School of Optoelectronic Information, Chengdu 610054, China
[b]University of Toronto, Center for Advanced Diffusion-Wave Technologies (CADIFT), Department of Mechanical and Industrial Engineering, Toronto M5S 3G8, Canada

Abstract. We used ultrasound (US) and photoacoustic (PA) imaging modalities to characterize cattle trabecular bones. The PA signals were generated with an 805-nm continuous wave laser used for optimally deep optical penetration depth. The detector for both modalities was a 2.25-MHz US transducer with a lateral resolution of ~1 mm at its focal point. Using a lateral pixel size much larger than the size of the trabeculae, raster scanning generated PA images related to the averaged values of the optical and thermoelastic properties, as well as density measurements in the focal volume. US backscatter yielded images related to mechanical properties and density in the focal volume. The depth of interest was selected by time-gating the signals for both modalities. The raster scanned PA and US images were compared with microcomputed tomography (μCT) images averaged over the same volume to generate similar spatial resolution as US and PA. The comparison revealed correlations between PA and US modalities with the mineral volume fraction of the bone tissue. Various features and properties of these modalities such as detectable depth, resolution, and sensitivity are discussed. [DOI: 10.1117/1.JBO.20.7.076016]

Keywords: photoacoustics; ultrasound; trabecular bone; quantitative ultrasound; osteoporosis; bone volume fraction; bone collagen content.

Paper 140620RR received Sep. 25, 2014; accepted for publication Jul. 2, 2015; published online Jul. 29, 2015.

1 Introduction

Bone is a complex three-dimensional (3-D) biostructure composed of both organic (mainly collagen Type I) and inorganic (hydroxyapatites) phases. The contributions of both parts are vital for bone integrity and proper functionality.[1–3] Although the bone mineral density (BMD) is definitely a major factor, bone strength and integrity are affected by many other factors as well. The shape and microstructure of the bone tissue as well as the bone composition (minerals versus organic parts) have enormous influence on how bones thrive.[2,4] While minerals can support compression stresses, collagen endures tensile stresses. Furthermore, collagen plays an important role in dissipating mechanical energy, which increases bone toughness and, therefore, reduces the risk of fracture.[1,3] It is no wonder that even a minor change in collagen molecule architecture, for instance, due to genetic diseases, can induce huge macroscale defects in bone.[1] Osteoporosis disease (OPD) is normally associated with a reduction in bone minerals, however, some research points to a correlation of fracture risk with changes in collagen content (CC) and collagen crosslinks.[2,5–7] Only a few studies have investigated the bone organic phase variation during OPD [8–10] and aging;[11,12] more research in this field is highly desirable.

Despite the ionizing radiation, dual-energy-ray absorptiometry (DXA or DEXA) measurements of BMD represents the current gold standard for OPD diagnosis and fracture risk assessment.[4] Quantitative ultrasound (QUS) is another choice for assessment of bone health. The QUS operating principle is based on the measurement of the speed of sound (SOS) and the normalized broadband ultrasound attenuation (nBUA).[13,14] Other methods based on the measurement of two waves or ultrasound (US) backscattering have also been proposed.[15–17] US backscattering from bone depends on the mechanical properties and the microstructure of the interrogated hard tissue,[17] which render it a good measure of bone health. US backscattering is normally represented by parameters such as backscatter coefficient,[18,19] broadband ultrasound backscatter (BUB),[20,21] integrated reflection coefficient,[22] and apparent integrated backscatter (AIB).[23–25] These parameters were extensively correlated with BMD or bone volume fraction (BV/TV) in the literature.[26]

Comparison between QUS images and BMD was also performed by Jenson et al.[27] BMD was obtained from x-ray quantitative computed tomography (QCT) and three different QUS parameters: SOS, nBUA, and BUB were measured at 1 MHz on 38 human trabecular bone samples. The above-mentioned QUS parameters were calculated on 7×7 mm^2 regions of interest (ROI) on the surface images and were compared with the corresponding ROI in QCT. Significant correlation was found between QUS parameters and BMD where the transmission-measured parameters (SOS and nBUA) demonstrate stronger correlation with BMD than the backscatter-measured parameter (BUB). In contrast to the extensive research reported on the QUS response to BMD variation, only a few authors have studied the effect of bone CC variation on QUS parameters.[28,29,21] It has been shown that SOS decreases and nBUA and AIB increase with decollagenization, although the correlations are weak.[28]

Recently, measurements of photoacoustic (PA) backpropagation from bones were reported for the first time.[30,31] Since PA is sensitive to the optical properties of tissue, it can detect composition variation and as such it can provide complementary

*Address all correspondence to: Bahman Lashkari, E-mail: bahman@mie.utoronto.ca

1083-3668/2015/$25.00 © 2015 SPIE

information to US backscattering measurements. In our previous studies, we showed the sensitivity of PA with changes in minerals and organic phases of bone.[32,33] We measured backpropagating US and PA signals on identical locations of bone samples before and after artificial demineralization and decollagenization.[33] In the present study, we used both US and PA to image the surface of trabecular bone samples in which half of the bone had been treated. Thus, the obtained raster scanned images were able to provide better insights of US and PA sensitivities to bone demineralization and decollagenization processes. Then the images were compared with microcomputed tomography (μCT) images of the samples, an independent well-established diagnostic analysis tool used as the gold standard in this context. In view of the very different spatial resolution scales, in order to correlate the μCT and the US-PA measurements, the μCT values were averaged over a rectangular cube. The square surface of the cube was chosen to correspond to the lateral resolution of the ultrasonic transducer, and the depth of the rectangular cube was selected according to the time-gated signal. The image comparison results confirmed the conclusions provided by individual point measurements about the sensitivity of US and PA modalities to demineralization and decollagenization.[33] The paper concludes with a discussion of the correlation of both US and PA measurements with the BV/TV derived from μCT.

2 Materials and Methods

2.1 *Bone Specimen Preparation*

Eight bone samples were harvested from the femurs of two cattle (Angus, Canadian) and cut into blocks. The samples were washed and then immersed and kept in saline solution for up to 2 days to wash out the blood and marrow as much as possible. The samples were then stored in a refrigerator before being treated or measured and were allowed to equilibrate thermally at room temperature prior to all experiments. The specimens were separated into two groups and during the experiments, they were treated with different agents to reduce their mineral or CC.[34–36,28] They were treated either with a 50% buffered solution of ethylenediaminetetraacetic acid (EDTA) (pH = 7.7) to demineralize the bone, or with a 5% solution of sodium liquid hypochlorite to reduce the CC.

2.2 *Experimental Setup*

The experimental setup is shown schematically in Fig. 1. It was designed to accommodate separate PA and US tests, as well as to perform multiple measurements before and after treatment at the same coordinate point of every sample.

Optical generation of PA signals was induced by a continuous wave 805-nm diode-laser (Laser Light Solutions, New Jersey). The laser driver was controlled by a software function generator for laser intensity modulation using a National Instruments DAC card PXI-5421 (National Instruments, Texas).

For the US experiments, a 3.5-MHz transducer (V382 Olympus NDT Inc., Panametrics) was used as the transmitter of modulated US. It was driven by a waveform generator identical to that of the laser driver. No power amplifier was required to boost the ultrasonic transmission due to the application of coded excitation.[37] A 2.25-MHz ultrasonic transducer (V305 Olympus NDT Inc., Panametrics) was used as the receiver with a 40-dB preamplifier (5676 Olympus NDT Inc., Panametrics) employed before the ADC card.

Signal acquisition was performed through a National Instruments PXI-5122 ADC card. To provide reference signals that represent the dynamics of the instrumentation (i.e., function generator, transducers, and preamp) regardless of the sample, the spectra of US reflection signals from a polished metal and PA backpropagating signal from a homogeneous absorber were obtained. The reference US and PA spectra are shown in Fig. 2 and were used later in the calculation of integrated US and PA parameters. More details about the experimental setup and signal analysis are described in our previous report.[31]

The chirp duration was 1 ms for both PA and US probes. However, different frequency sweeps were used for the two modalities. The frequency range employed for the PA chirp was 300 kHz to 2.6 MHz and for the US chirp was 300 kHz to 4 MHz. The rationale for these frequency sweeps was to maximize the signal-to-noise ratio (SNR).[38] The reference signals (Fig. 2) show the sensitivities of the implemented PA and US system versus frequency and justify the optimal frequency range selected for each modality. The US transmitter element was selected based on obtaining the same lateral resolution in the focal point as the receiver transducer. Both transducers had approximately identical focal zone widths of ~1 mm (0.87 mm and 0.9 mm for transmitter and receiver,

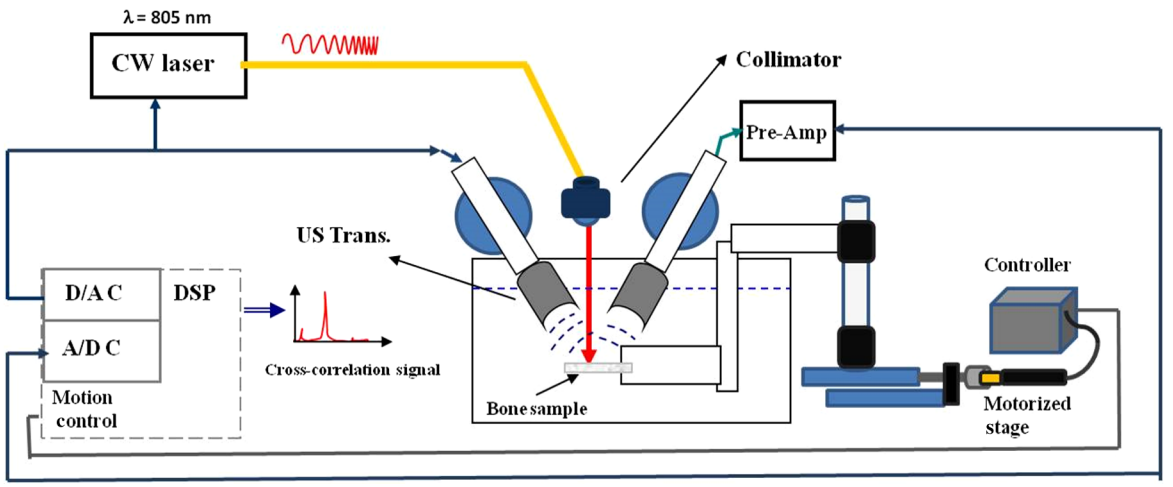

Fig. 1 Experimental setup.

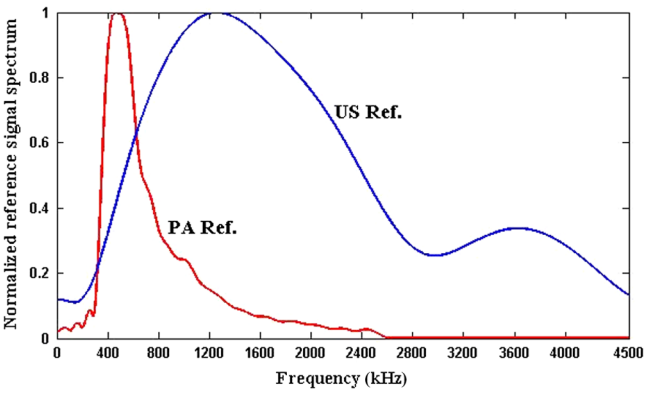

Fig. 2 Reference photoacoustic (PA) and ultrasound (US) spectra. The US reference signal was obtained from reflections from a polished metal and the PA reference signal was obtained from backpropagation from a homogeneous absorber.

respectively).[39] Also, the size of the element was a critical factor. The diameter of the transmitter was 0.5 in., smaller than the 0.75 in. for the receiver. The center frequency was the second priority. Both of the transducers were wideband and covered the chirp frequency ranges. As a result, the sensitivity of the US measurements was reasonably good and it did not even require power amplification as mentioned before.

To perform accurate and fast raster scanning over the bone surface, a step motor and its DC servo controller (PT1-Z8 and TDC001, Thorlabs) were employed. The signal generation, acquisition, and servo controller were controlled by an in-house developed LabView program (National Instruments, Texas), which allowed for synchronization between signal generation and acquisition. The motor was used to scan the sample in steps of 1 mm. A total of 20 points were interrogated on each scanned line. Displacement in the other (vertical) direction was effected manually using a micrometer stage.

To identify the boundary between the treated and the intact parts of bones, two holes were drilled on their surface serving as landmarks. A screw was attached to the bone far from the measurement zone and was used to fix the bone to the stage for measurements and to allow for hanging the sample over the solution for partial immersion. The samples were immersed either in the demineralization or in the decollagenization solution so that the landmarks were located at the level of the solution–air interface, as shown in Fig. 3(b). These landmarks, as well as additional artificially made landmarks, were also used in identifying the exact points during μCT and for measurements at specific points on the surface of the bone before and after the various treatments [Fig. 3(c)].

μCT is a well-established bone assessment method, which has been used to validate the US and PA backpropagated signal correlation to BV/TV. These comparisons can highlight differences and the degree of complementarity between modalities. The samples were scanned using the commercial system (μCT 40-Scanco Medical AG, Brüttisellen, Switzerland). For each bone, between 898 and 1933 μCT, signal slices were generated depending on the length of the bone. Virtual image slices were produced using an 18-μm stepsize with a 18-μm pixel resolution at each slice. The slices were then converted to two-dimensional Digital Imaging and Communications in Medicine (DICOM) images, which were analyzed by an in-house developed MATLAB program. The MATLAB program first generates a 3-D matrix characterizing the 3-D bone

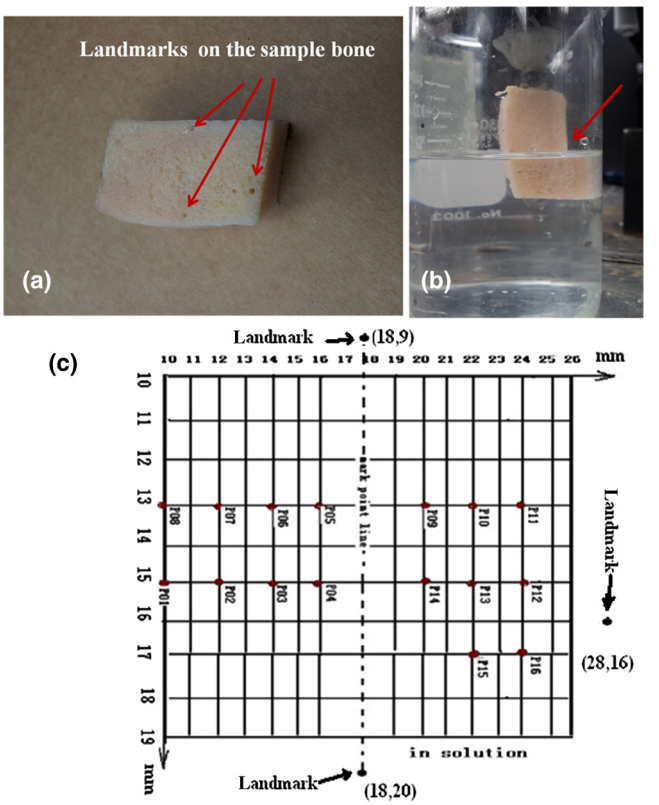

Fig. 3 Landmarks were artificially made to distinguish the measurement points and mark the horizontal line below which the sample was immersed in the solution agent. (a) Three demarcation points on the sample; (b) demarcation line coincides with the solution surface; and (c) the relative position of the 16 measured points with respect to the landmark line on one sample

model based on the μCT slices. Then the planes rotate in three directions to adjust the direction to the measured surface and the program adjusts the matrix accordingly. At this stage, it is possible to calculate the BV/TV at any subvolume of the matrix and compare it with measurements. The high resolution of μCT enables very accurate assessment of BV/TV in very small volumes. However, the lateral resolution of US and PA signals is limited to the lateral resolution of the transducers which, in our case, was $\sim$1 mm. Our MATLAB program performs averaging over a volume of 1 mm $\times$ 1 mm (on the surface) $\times$ 4 mm (in depth). The time-gating process allows the extraction of the part of the signal corresponding to this depth and the square area corresponds to the lateral resolution of the detection system. Thus, the averaged BV/TV in this volume also corresponds to the measured US and PA signals.

Decollagenization was performed using sodium hypochlorite solutions (NaOCl) with 5% concentration and was applied for 3 h. EDTA 50% was used as a demineralization solution and was applied for 5 h. After the designated time, the sample was washed and measurements were performed again. The four samples which were demineralized with the EDTA solution will be henceforth labeled 1a, 2a, 3a, and 4a. The other four samples, which were decollagenized through treatment with the sodium hypochlorite solution, will be labeled 1b, 2b, 3b, and 4b.

It is informative to provide an evaluation of the extent of demineralization and decollagenization. Figure 4 shows the μCT cross-sectional images of samples 1a and 1b at 2 mm

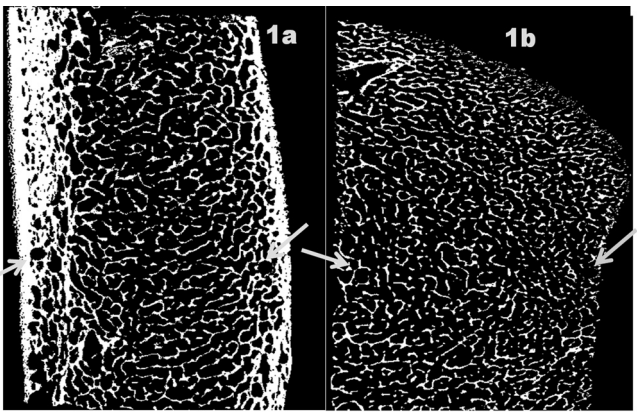

Fig. 4 Microcomputed tomography (μCT) sectional images of samples 1a and 1b (2 mm beneath the surface), partially demineralized and decollagenized, respectively. Arrows point to the landmarks on the surface of the samples.

beneath the surface after the treatments. Parts of these samples below the landmarks were demineralized and decollagenized, respectively. It is very difficult to visually distinguish the small reduction in the trabeculae of sample 1a. The effect of demineralization was readily quantified by employing the results of μCT. As discussed, the volume fraction of minerals and its correlation with PA and US signals is a major part of this study. Here, the degree of artificial demineralization is shown in Table 1. This table shows the percentage of difference in the BV/TV of treated versus intact parts of the samples. It can be seen that on average, the BV/TV of the demineralized samples is 21.9% less than that of the intact parts of the same samples. On the other hand, the average BV/TV of the decollagenized samples is 6.5% less than that of the intact parts of the same samples. The evaluation of the extent of decollagenization is not as easy as in the demineralization case because it requires destructive methods. Therefore, the CC assessment was performed after completing all the other measurements. A hydroxyproline assay kit (# 6017, Chondrex, Inc., Redmond, Washington) was employed to evaluate the CC of the bone samples. A few small bone parts were cut off from each bone surface (at the location of measurements) with a surgical blade. Bone parts were mashed, powdered, and left to dry. For each part of the samples, ~10 mg of bone tissue (powdered) were poured into a glass screw-capped vial. About 100 μl of distilled water and 100 μl of concentrated hydrogen chloride (10N) were added to the vial and the Teflon cap was tightened. The same sample preparation process was performed for treated and intact parts of all samples (all in duplicate). Then all the vials were marked and kept on a hot plate at 120°C for 16 h. The vials were shaken regularly during the incubation time. After finishing the hydrolysis process, the samples were arranged in the 96-well plate. A set of standard dilutions of hydroxyproline were also prepared according to the kit instructions and were deployed in the first two columns of the plate. A plate reader was used to obtain the optical density (OD) probed with 550-nm wavelength. The ODs of the standard samples were used to generate a curve relating OD readings versus hydroxyproline levels. Using this curve, the hydroxyproline levels and, therefore, the collagen levels of the samples were estimated. This led to the calculation of the CC of the samples. Table 1 shows the percentage of the change in the CC of the treated versus intact parts of the bone samples. It can be seen that on average, the CC of the decollagenized samples is 32% lower than that of their intact parts. The CC of the demineralized samples is 6.8% higher than their intact parts.

As mentioned before, several factors besides minerals and CC can affect the PA and US signals. One important factor is the alignment and anisotropy of trabeculae. Since μCT measurements of the samples were available, assessment of the alignment and anisotropy was feasible. One quantitative and accurate method for assessing these factors is the use of a Gabor filter. The procedure is described elsewhere,[40] and briefly explained here. The ROI is selected from a μCT slice 2-mm beneath the surface from each part of the bone samples: treated and intact. The Gabor filter was applied to the μCT slice by 10 deg rotational steps. Plotting the results in different directions

Table 1 The extent of demineralization and decollagenization of samples, as well as their degree of anisotropy (DA).

		Extent of Demineralization [%]	Extent of Decollagenization [%]	DA	
				Intact	Treated
Demineralizated samples	la	−20.5	14.7	1.93	1.59
	2a	−17.7	−7.8	1.33	1.36
	3a	−30.5	13.1	2.8	1.73
	4a	−16.6	7.1	2.10	1.95
Average:		−21.9	6.8	2.04	1.66
Decollagenized samples	1b	−7.7	−37.3	1.49	1.86
	2b	−4.4	−22.1	1.73	2.2
	3b	−9.0	−13.5	1.55	3.32
	4b	−3.6	−55.2	1.82	1.64
Average:		−6.5	−32.0	1.65	2.25

provides a directionality map of the μCT slice. Figure 5 shows four selected ROIs from samples 1a and 1b. Besides each μCT section, its calculated directionality map is also displayed. These directionality maps can help identify the main directionality in each part of the bones. Furthermore, they can also be used to calculate the degree of anisotropy (DA) of the trabeculae.[41] The DA of all samples is reported in Table 1. The directionality and DA can affect the US and PA signals. The extent of the effect of directionality on the backscattered signal can be estimated from previous studies, where it was shown that the US backscattering coefficient is 1.8 dB lower in the anteroposterior (AP) than the mediolateral (ML) direction in human calcaneus at 500 kHz. Another *in-vitro* study showed that the US apparent integrated backscatter is less than 1 dB lower in AP and superoinferior directions compared with the ML in bovine tibia in the 1 to 3 MHz frequency range.[17] These studies measured the US backscatter signal in completely different directions. In our study, the measurements were performed on two adjacent parts of the same samples; therefore, the effect of directionality was expected to be lower.

2.3 *Experimental Verification of Water Absorption Effects on the Ultrasound and Photoacoustic Signals*

For the sake of consistency in the results, we used a measurement method (protocol) similar in all experiments, which was also similar to our previous studies.[31,33] We performed the measurements after letting the bone samples soak in saline solution for 2 h to be degassed.[16] Therefore, it was important to investigate if water permeation had any significant effect on our PA and US measurements. We performed repetitive PA and US measurements at eight points on one sample (sample 1a) while it was immersed in saline solution. The sample remained in the solution for 10 h and the measurement was repeated every 2 h. Figure 6 shows the variation of PA and US signals at one location due to water immersion and soaking. It can be observed that the first peak changes (due to reflection) are only minor. The later peaks show some variation, however, the location and number of these peaks remain mostly unchanged. It should be noted that in the calculation of US AIB, the first peak is eliminated by time gating, but it is considered in the calculation of PA AIB. Figure 6(c) shows the average variation of the calculated AIB at 15 points during 10 h of immersion. The figure shows that the variation of PA and US AIB due to water absorption is much smaller than the variation due to position change on the bone surface. It should be mentioned that the samples were not dried after preparation and storage in the refrigerator. Therefore, the experimental results show the effect of changes following sample immersion in water for several hours.

2.4 *Ultrasound and Photoacoustic Imaging of Bones*

In the half-immersed sample geometry of Fig. 3, PA and US measurements were performed on the entire zone, as described in Sec. 2.2. Surface images are not only used for technique sensitivity assessment to bone decollagenization and demineralization, but also are very helpful for studying correlations with the corresponding μCT images. The comparison method is explained below. As shown in Fig. 3, several coordinate points on both sides of the boundary line landmarks were selected and measurements were performed before and after each treatment. Signal variance on the intact part of the bone reveals deviations due to factors other than decollagenization and/or demineralization.

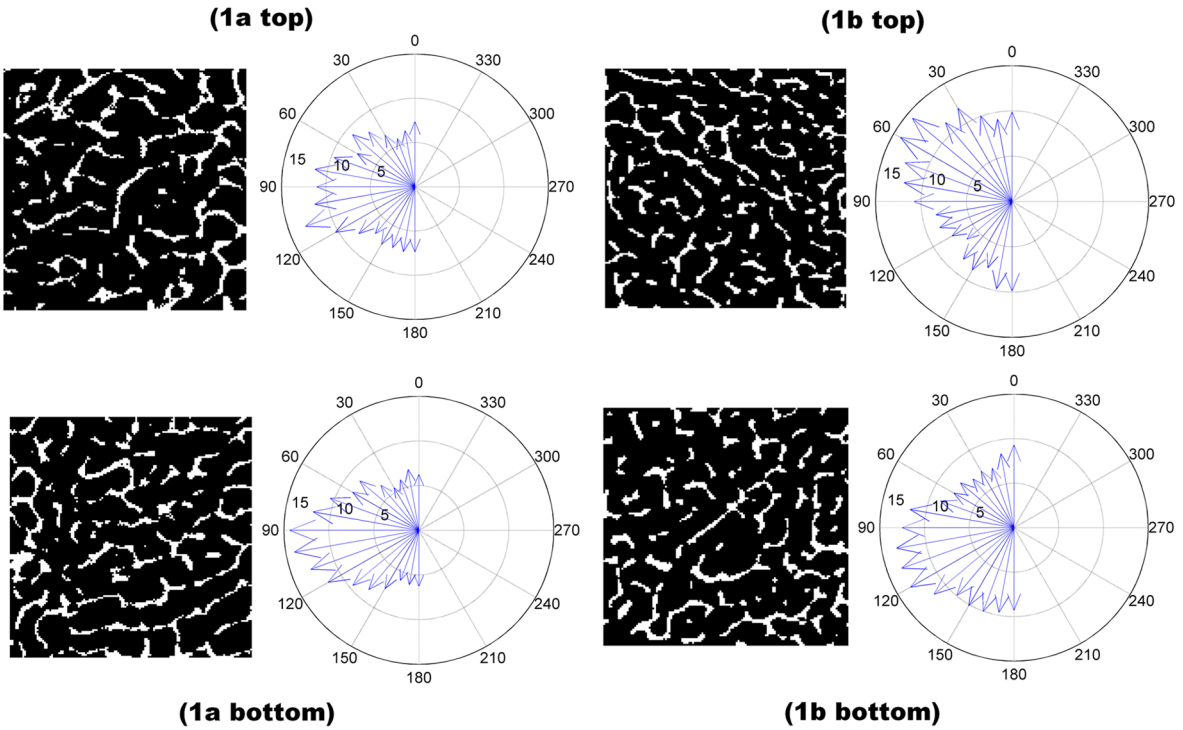

Fig. 5 Selected areas of μCT sectional images of samples 1a and 1b (Fig. 4) and their corresponding directionality maps. These maps display the directionality and degree of anisotropy of the treated and intact parts of the bone samples.

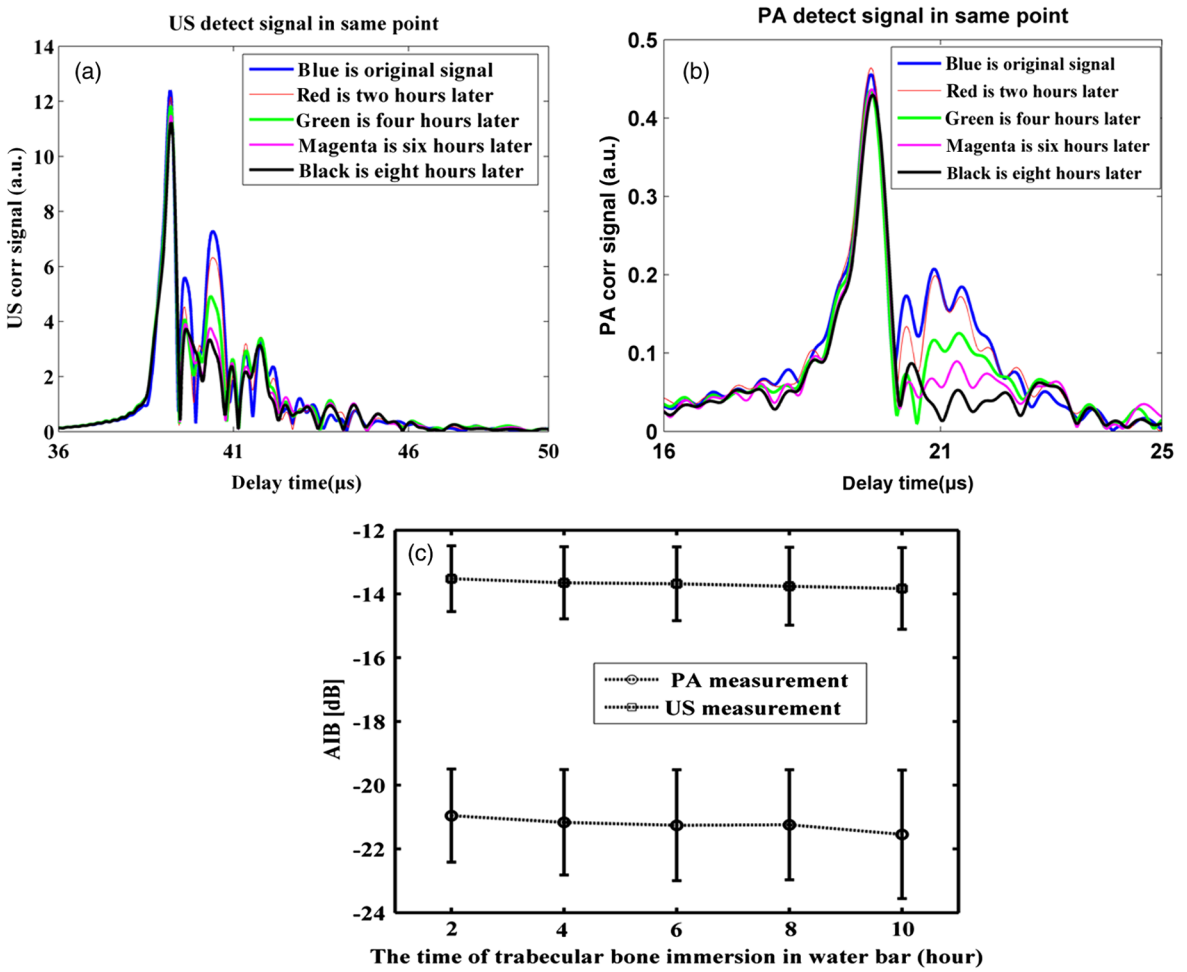

Fig. 6 PA and US cross-correlations at one point for five consecutive measurements. The sample remained in water for 10 h and the measurement was repeated every 2 h. (a) US cross-correlation; (b) PA cross-correlation; (c) the averaged PA and US apparent integrated backscatter (AIB) values of 15 points during the five consecutive measurements.

The tested hypothesis was that other variations should be statistically insignificant compared to those incurred by decollagenization and/or demineralization. Eight or nine points on each half side of all samples were selected so that the distance between points, as well as between each point and the solution boundary, was at least 2 mm.

2.5 *Image Analysis*

Scanning experiments of US and PA back-propagating signals of all eight trabecular bone samples were performed. For proper comparison among the three measurement modalities (US, PA, and μCT), a quantitative analysis of PA and US experimental results was made as follows: AIB value images present the variation in the normalized signal for the treated and intact parts of the samples. The AIB[24,31] was determined by frequency averaging (integrating) the ratio of the power spectrum of the time-gated signal (P_b) to the power spectrum of a reference signal (P_r) (Fig. 2) over the chirp frequency range:

$$\mathrm{AIB} = \frac{1}{\Delta f}\int_{\Delta f} 10\log_{10}\left[\frac{P_b(f)}{P_r(f)}\right]df. \quad (1)$$

Next, with regard to the US reference spectra (Fig. 2), it can be seen that the AIB calculation is weighed more toward the high frequency range of the signal spectrum than the middle range because of the division in Eq. (1). To normalize the frequency response, it is possible to apply a counter-weighing filter to AIB to offset the low components at the edges of the frequency range. However, since all of the signals in this investigation used the same set-up and laser/US intensity, the frequency-averaged power spectrum of the signal can be used for comparison. Similar to AIB, time gating was applied to extract the signal corresponding to backscattering down to a certain depth. Integrated-power images represent the overall variation of the backscattered signal power with and without treatment. To present the power in dB, normalization with the integrated-power spectrum of the reference signals (Fig. 2) was made and yielded the normalized apparent backscattered (NAB) signal, defined as

$$\mathrm{NAB} = 10\log_{10}\left(\frac{\int_{\Delta f} P_b(f)df}{\int_{\Delta f} P_r(f)df}\right). \quad (2)$$

The values of AIB and NAB for both US and PA modalities were compared with the BV/TV from μCT. Also the correlations of these two modalities were compared with each other.

Depthwise images perpendicular to the boundary between intact and treated bone sectors presented some interesting features for comparison between PA and US modalities, which will be discussed below. The μCT image slices were averaged over the $1 \times 1 \times 4$ mm^3 volume as described before from the same assessed surface of the bone. These images present the BV/TV within the volumes corresponding to the US and PA images. Image correlations reveal relative sensitivities of these modalities to BV/TV as well as signal dependencies on other factors.

3 Results

Figure 7 shows several images of the partly demineralized sample 1a. A photograph of the sample is shown in Fig. 7(a), with a box indicating the scanned area. Figure 7(b) is a μCT image generated by adding 223 slices corresponding to the 4-mm depth. The PA and US AIB images show the variation of PA backpropagation and US backscatter (AIB) within the scanned region, Figs. 7(c) and 7(d), respectively. Corresponding PA and US NAB images are shown in Figs. 7(e) and 7(f), respectively. The depth profile cross-sections generated by the PA and US

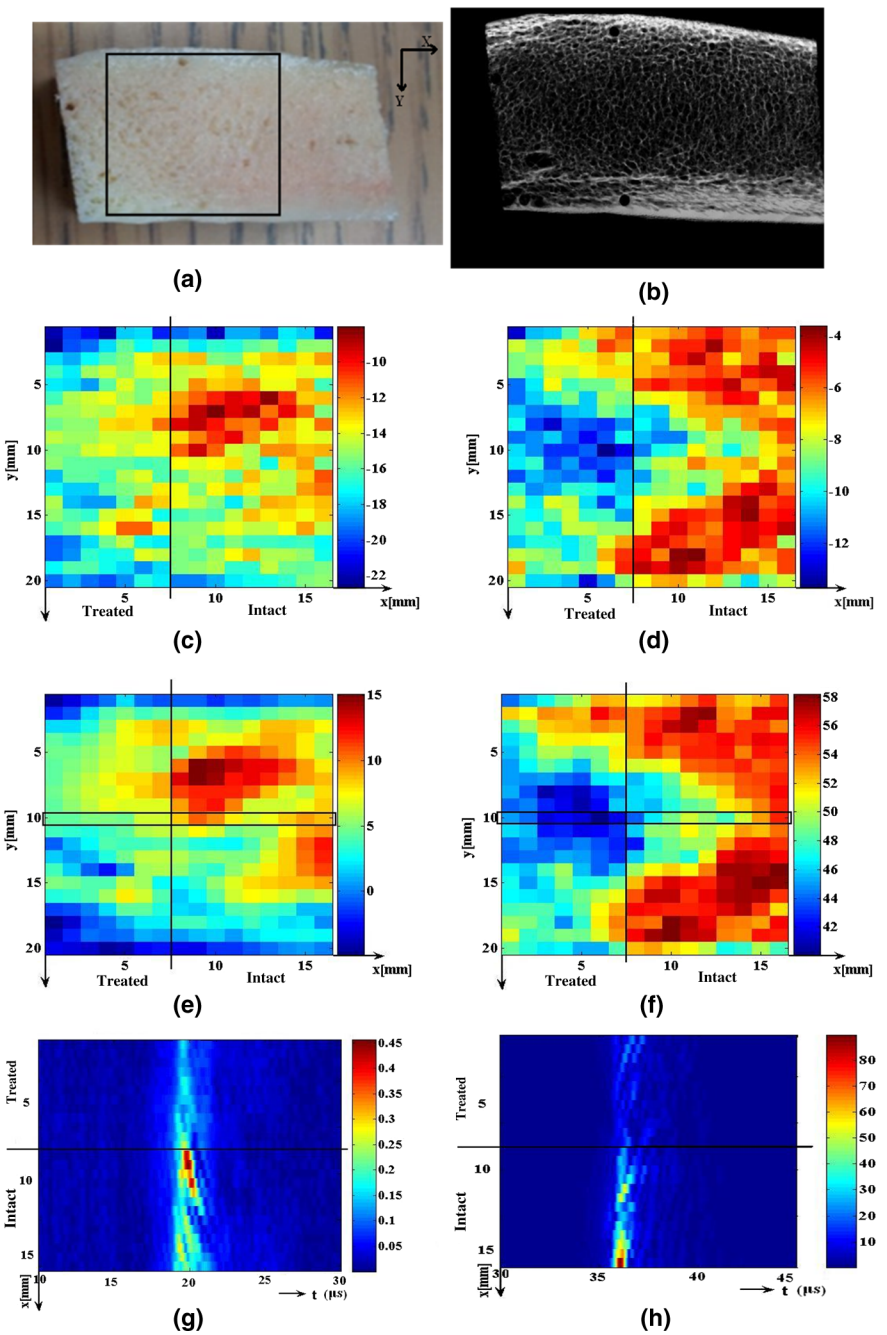

Fig. 7 Partially demineralized sample 1a: (a) photograph; (b) 4-mm collected μCT slices. Scanned images: (c) PA AIB; (d) US AIB; (e) PA normalized apparent backscattered (NAB); (f) US NAB; (g) PA image cross-section; and (h) US image cross-section. The location of cross-section images corresponds to the line box shown in (e) and (f).

cross-correlation functions are presented in Figs. 7(g) and 7(h), respectively; they show the signal attenuation profiles with delay time. It should be noticed that delay time corresponds to depth. The surface coordinates of the presented cross-sections are shown as thin horizontal bars in the NAB images, Figs. 7(e) and 7(f). The vertical line in the middle of each image represents the abovementioned landmark line, which was used to distinguish treated and intact sample halves.

Figure 8 is the counterpart of Fig. 7 with respect to sample 1b, which was partly decollagenized and they appear in the same order as Fig. 7. Figure 9 is a histogram of the surface-averaged PA and US AIB variations produced by point measurements on the treated and the intact parts of the bone samples before and after treatment. These variations show the sensitivity of each modality to decollagenization and demineralization. Figure 9 shows the reproducibility of the experiments, where the points in the intact part of the bone show very small variations.

4 Discussion

Figure 7 presents the surface scanned images of the partly demineralized sample 1a. It can be seen that the PA and US AIB and NAB exhibit significant changes in the demineralized half compared with the intact half of the bone. Similarly, in the depth profiling images, the reduction of both PA and US signals is evident. In this study, PA and US AIB were both found to significantly decrease with BV/TV reduction. This result is

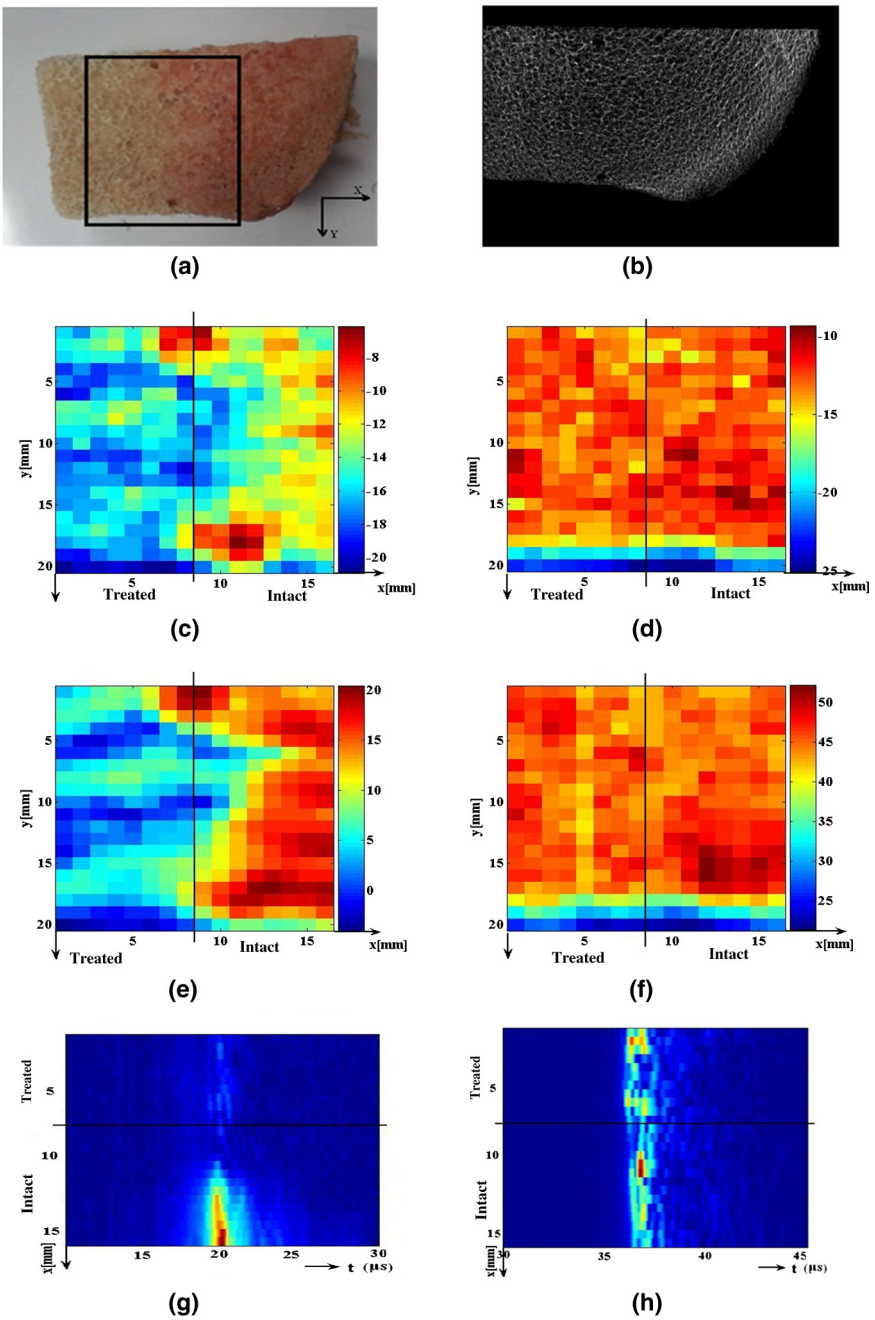

Fig. 8 Partially decollagenized sample 1b: (a) photograph; (b) 4-mm collected μCT slices. Scanned images: (c) PA AIB; (d) US AIB; (e) PA NAB; (f) US NAB; (g) cross-section PA; and (h) cross-section US image.

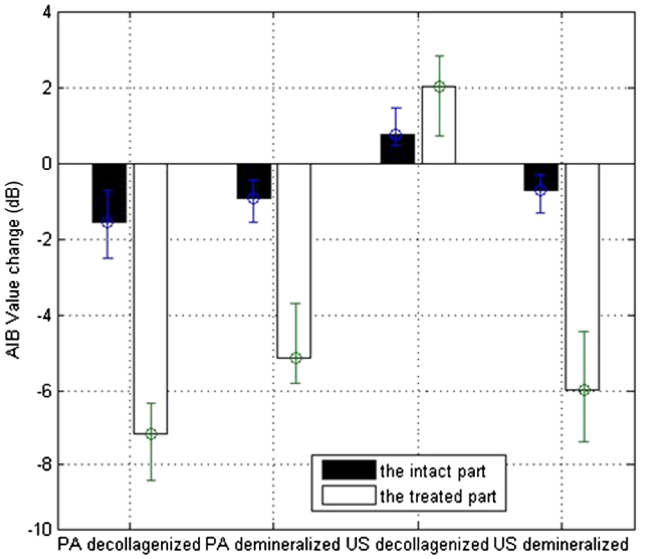

Fig. 9 PA and US AIB value variation histogram before and after treatment for intact and treated parts of the bone samples.

consistent with previous reports where both modalities show sensitivity to changes in BV/TV of trabecular bone with US having higher sensitivity.[31,33]

Figure 8 presents the AIB and NAB scanned images of the partly decollagenized sample 1b. It is observed that the PA AIB decreased significantly after decollagenization, whereas the US AIB increased slightly. The consistency of these results with the other tested samples is addressed in the discussion of Table 2, where the average change of parameters for each sample and the total average over all samples are presented. The depthwise images also show a clear reduction of the PA signal in the decollagenized part of the sample, Fig. 8(g).

In Table 1, we show the extent of demineralization and decollagenization of the samples. The average differences of BV/TV of the treated and intact parts for demineralized and decollagenized samples are 21.9% and 6.5%, respectively. Furthermore, the average difference of CC of treated and intact parts for decollagenized samples is 32% less and for demineralized samples is 6.8% higher. These differences are reasonable and agree with the agents employed for treatment of the bone samples. Additionally, they support our conclusions on the effect of demineralization and decollagenization on US backscattering and PA backpropagating signals. The average differences of AIB and NAB parameters between the treated and intact parts of all bone samples are presented in Table 2. This table also shows the averaged BV/TV of the ROIs in the treated and intact parts of the bone samples.

The AIB and NAB values for all samples (Table 2) as well as the average changes (Table 1) show the consistency of the foregoing results for samples 1a and 1b with the remaining samples: both PA and US parameters (AIB and NAB) were reduced significantly in the demineralized part of the bone. PA signals were reduced significantly in the decollagenized part of the bone, while US parameters increased slightly in the decollagenized part. The behavior of US backscatter parameters is consistent with the QUS literature, where the slight increase of US backscattering with decollagenization is interpreted to be due to the decrease in acoustic wave attenuation.[28] Table 2 also reports the correlation coefficient between the PA and US parameters. It can be seen that PA and US parameters exhibit weak-to-moderate correlations for the demineralized samples, as they both respond fairly similarly to demineralization treatment. The NAB parameter shows stronger correlation between the two modalities. As discussed later on, the NAB parameter also correlates better with BV/TV. On the contrary, the PA and US parameters exhibit no correlation for the decollagenized samples. This can be understood by considering the different responses to reduction of CC by the two modalities: the US backscattering is affected by a decrease in attenuation, whereas the PA backpropagation is affected by the reduction in chromophore (absorber) density.

Table 2 The correlation coefficient between US and PA parameters as well as difference between the AIB and NAB and bone volume fraction in treated and intact parts of the bones.

		Difference between treated and intact bone [dB]				US-PA correlation		BV/TV	
Sample		US AIB	PA AIB	US NAB	PA NAB	AIB	NAB	Intact	Treated
Demineralized samples	1a	-4.96 ± 3.36	-2.86 ± 2.54	-5.99 ± 4.02	-6.17 ± 2.68	0.250	0.206	0.215	0.171
	2a	-2.28 ± 1.56	-2.29 ± 2.02	-4.84 ± 3.19	-2.43 ± 1.84	0.333	0.525	0.254	0.209
	3a	-2.61 ± 1.24	-4.38 ± 3.53	-6.16 ± 3.03	-6.92 ± 1.86	0.358	0.561	0.269	0.187
	4a	-3.31 ± 2.52	-3.78 ± 3.27	-3.59 ± 2.83	-4.02 ± 3.15	0.361	0.436	0.193	0.161
Average:		-3.29 ± 2.32	-3.33 ± 2.9	-5.15 ± 3.3	-4.88 ± 2.45	0.326	0.432	0.233	0.182
Decollagenized samples	1b	1.63 ± 1.92	-5.24 ± 1.73	3.74 ± 3.89	-5.81 ± 1.77	−0.405	−0.043	0.234	0.216
	2b	1.02 ± 1.49	-3.04 ± 2.97	0.22 ± 2.05	-5.64 ± 2.82	−0.318	−0.126	0.183	0.175
	3b	1.92 ± 1.32	-3.61 ± 2.25	2.81 ± 1.96	-4.22 ± 1.54	−0.584	−0.165	0.221	0.201
	4b	1.40 ± 1.99	-6.27 ± 1.95	0.52 ± 2.12	-6.23 ± 2.08	−0.344	−0.143	0.165	0.159
Average:		1.49 ± 1.7	-4.54 ± 2.27	1.82 ± 2.63	-5.48 ± 2.11	−0.413	−0.119	0.201	0.188

Table 3 The correlation coefficient between US or PA NAB and microcomputed tomography (μCT) in the treated and intact parts of the samples.

		Intact part		Treated part	
		US/μCT	PA/μCT	US/μCT	PA/μCT
Demineralizated samples	1a	0.532	0.325	0.437	0.148
	2a	0.757	0.388	0.532	−0.021
	3a	0.743	0.554	0.353	0.199
	4a	0.683	0.371	0.469	0.162
Average:		0.679	0.409	0.448	0.122
Decollagenized samples	1b	0.756	0.392	0.821	−0.264
	2b	0.680	0.397	0.712	−0.309
	3b	0.607	−0.502	0.698	−0.189
	4b	0.548	0.287	0.473	−0.086
Average:		0.648	0.144	**0.676**	**−0.212**

Table 4 The correlation coefficient between average US or PA AIB and μCT in the treated and intact parts of the samples.

		Intact part		Treated part	
		US/μCT	PA/μCT	US/μCT	PA/μCT
Demineralized samples	1a	0.518	0.433	0.285	0.262
	2a	0.577	−0.112	0.567	−0.367
	3a	0.309	−0.125	−0.283	−0.183
	4a	0.632	0.327	0.375	0.052
Average:		0.509	0.131	0.236	−0.059
Decollagenized samples	1b	0.490	0.358	0.312	−0.085
	2b	0.487	0.436	−0.536	−0.486
	3b	0.322	0.146	0.264	0.137
	4b	0.511	0.233	0.394	−0.078
Average:		0.453	0.293	0.108	−0.128

The correlation coefficients between US or PA NAB and BV/TV (derived from the μCT images) in the treated and intact parts of the samples were calculated separately and are shown in Table 3. A moderate linear correlation between US NAB and BV/TV was found for the intact parts of all samples, with r values from 0.532 to 0.757. A weak correlation between PA NAB and BV/TV was found for the intact parts of all samples. The correlation coefficient between US NAB and BV/TV slightly decreased after demineralization. On the contrary, the correlation between US NAB and BV/TV slightly increased after decollaganization. This can be understood by considering that the main effect of the organic parts of the bone on the US signal is attenuation, so that by decreasing the volume fraction of minerals, the US signal attenuation is affected the most. On the other hand, by decreasing the CC, the attenuation component due to the collagen reduces and the US signal correlation with mineral content is expected to increase. The correlation of PA NAB and BV/TV decreased after both treatments. Similarly, the correlation coefficients between US or PA AIB and BV/TV in the treated and intact parts of the samples are calculated and reported in Table 4. The correlation between the US AIB and BV/TV is weak-to-moderate for the intact parts of all samples, with r values from 0.309 to 0.632, which are relatively small compared with those between the US NAB and BV/TV. Also, the PA AIB shows weak correlation with BV/TV after either treatment.

Table 5 shows the correlation coefficients for the measured parts of the bone (both treated and intact) with the corresponding BV/TV calculated from μCT. This table summarizes the main results of this study. It can be seen that US NAB generates a moderate correlation with BV/TV for the demineralized samples, whereas US AIB shows a weak correlation for these sets of samples. Therefore, NAB seems to be a superior parameter for assessment of trabecular bone. US NAB also shows weak correlation with BV/TV for the decollagenized samples. The PA NAB shows a weak correlation with BV/TV for the demineralized part of the sample. On the other hand, the PA parameters (NAB and AIB) do not show any correlation with BV/TV for decollagenized samples. To understand these results, it should be kept in mind that US backscatter is not a sole function of bone density. As mentioned before, other parameters such as random structure and anisotropy of the trabeculae can affect it by causing multiple scattering and ultrasonic beam distortion.[42] From Table 1, it can be calculated that on average, there is a 22.6% difference in the DA of the two adjacent parts of the bone samples. Similar differences in DA also existed in the various locations where the measurements were performed. These factors can limit strong correlations of US

Table 5 The correlation coefficient between μCT and PA/US AIB including both treated and intact parts of the samples.

		AIB		NAB	
		US/μCT	PA/μCT	US/μCT	PA/μCT
Demineralized samples	1a	0.263	0.324	0.514	0.421
	2a	0.442	−0.353	0.579	−0.433
	3a	0.382	0.546	0.751	0.607
	4a	0.513	0.289	0.631	0.348
Average:		0.400	0.201	0.619	0.236
Decollagenized samples	1b	0.358	0.312	0.724	0.370
	2b	−0.373	0.658	−0.448	0.683
	3b	0.342	−0.255	0.698	−0.378
	4b	0.424	0.187	0.592	0.225
Average:		0.188	0.226	0.391	0.225

backscatter parameters with BV/TV. They are more effective at frequencies above 1 MHz where ultrasonic wavelength is on the order of trabecular dimensions, therefore, a lower correlation should be expected in comparison with similar studies, such as Jenson et al.,[27] who used 1 MHz for their studies. For PA parameters, in addition to those factors, the molecular composition of the sample should also be considered; thus, it would be logical to expect weaker correlation for PA with BV/TV than for US signals.

The averaged correlation coefficients show that NAB provides better correlation than AIB with μCT and it is consistent for all cases of demineralized samples for both PA and US modalities. It should be noticed that in the NAB calculation, no spectral weighing was applied in postprocessing. Spectra are weighed automatically with the transducer transfer function, the PA energy conversion, and other elements of the transfer function involving the instrumentation. Therefore, noise does not increase in postprocessing. In the calculation of AIB, normalization with the reference signal spectrum applies a weighing function that enhances signal components at the frequency margins of the spectra where the SNR is small, thereby boosting noise. Additionally, the NAB contains more low-frequency content compared with the AIB due to the lack of the aforementioned artificial weighing, as can be seen in the reference spectra. These two factors justify the fact that NAB is a better metric for evaluation of US and PA backpropagation signals.

Figure 9 shows the average changes of PA and US AIB with demineralization and decollagenization. The filled columns show the changes of this parameter in intact bone in measurements before and after exposure to the solution. Thus, the filled columns define the variation baseline of PA and US AIBs due to changes in consecutive measurements without any treatment of the bone tissue. These "before" and "after" treatment results are similar to our previous studies[32] and are consistent with the images presented in Figs. 7 and 8 for treated and intact parts of the bone.

The main purpose of this study was to examine the sensitivity of PA and US to variations in mineral and CC of the trabecular bone. Employing surface imaging on treated versus intact parts of bone samples provides a better understanding of the bone condition compared with random single-point measurements. In the presented experiments, single-element transducers were employed to maximize sensitivity. It is beneficial to use a customized designed array transducer matching the skeletal site under study for fast clinical application. However, a prerequisite to that stage is to establish AIB and NAB thresholds for reliable osteoporosis diagnosis.

One limitation of this study is that all the measurements were performed *in vitro*. Therefore, it is unknown how *in vivo* tissue and cortical bone overlayers, as well as the presence of marrow, can affect the results. However, our previous experiments demonstrate the possibility of PA signal detection under a 1.5-mm-thick cortical layer.[31] Similarly, other authors also reported the possibility of PA imaging under the skull layer.[43,44] To mitigate errors due to the presence of soft tissue and cortical layer in QUS, dual-frequency ultrasound has been suggested.[45,46] In those applications, measurements at two different frequencies were used to enable sufficient precision despite the existence of those overlayers. With the PA modality, one may not only use different frequency ranges but also multiple wavelengths, which is a major capability when it comes to increasing accuracy.

5 Conclusions

In this study, we introduced a volumetric correspondence between the US backscattered and PA backpropagation parameters, and the μCT calculated BV/TV. The resolution of all modalities was numerically adjusted so that it would be similar for all three modalities. We also defined a modification for the AIB in QUS, which we named as NAB. Similarly, this parameter was also defined for PA detection and we showed that for wideband detection, it correlated with BV/TV most closely. This is due to omitting the synthetic weighting of the spectra, which sacrifices SNR. It may not be very important for limited bandwidth detection, but the effect was crucial for wideband detection.

In conclusion, our findings provide insights into PA and US modalities in which PA and US AIB and NAB values were found to decrease with demineralization (decreases in BV/TV), but they exhibit opposite trends with changes in CC, with PA signals being more sensitive to those changes: US signals increase and PA signals decrease with decreasing CC. The findings about US backscattering with demineralization and decollagenization are consistent with the QUS literature. As mentioned before, there exists a large body of literature on the US backscattering relationship with BMD,[17,23,24,26,27] while only few studies have been reported on its relation to CC.[28,29,21] In the QUS literature, the relation between US backscattering and CC is attributed to acoustic attenuation. PA backpropagation analysis is novel and reports in the literature are limited to this and our previous studies. From the present studies, it is concluded that PA and US raster scan images over portions of bovine bone samples exhibit weak and moderate correlations with BV/TV, respectively.

Considering that the prevailing OPD diagnostic methods, such as DEXA, are only BMD specific, a combination of PA and US probes may result in improved sensitivity and specificity for the detection of bone demineralization or decollagenization, leading to more accurate bone loss diagnosis.

Acknowledgments

The authors gratefully acknowledge the support of the Canada Council for the Arts through a Killam Fellowship to A. M. They also acknowledge the help of professor J. E. Davis and Dr. Elnaz Ajami (IBBME, University of Toronto) in performing the μCT of the bone samples. The authors thank Dr. Amir Manbachi (IBBME, University of Toronto) for helpful discussions in finding the anisotropy of the samples as well as Mr. Shendu Ma (MIE, University of Toronto) for his help with hydroxypropline assay of the samples. Lifeng Yang is grateful to project Grant No. 2014HH0064 supported by Sichuan Provincial International Cooperation and Young Teachers Abroad (Habitat) plan of the UESTC.

References

1. M. E. Launey, M. J. Buehler, and R. O. Ritchie, "On the mechanistic origins of toughness in bone," *Annu. Rev. Mater. Res.* **40**, 25–53 (2010).
2. S. Viguet-Carrin, P. Garnero, and P. D. Delmas, "The role of collagen in bone strength," *Osteoporosis Int.* **17**, 319–336 (2006).
3. R. O. Ritchie, M. J. Buehler, and P. Hansma, "Plasticity and toughness in bone," *Phys. Today* **62**(6), 41–47 (2009).
4. G. M. Blake and I. Fogelman, "Technical principles of dual energy X-ray absorptiometry," *Semin. Nucl. Med.* **27**, 210–228 (1997).
5. P. Garnero, "The contribution of collagen crosslinks to bone strength," *BoneKEy Rep.* **1**, 182 (2012).

6. M. Saito and K. Marumo, "Collagen cross-links as a determinant of bone quality: a possible explanation for bone fragility in aging, osteoporosis, and diabetes mellitus," *Osteoporosis Int.* **21**, 195–214 (2010).
7. X. Wang et al., "The role of collagen in determining bone mechanical properties," *J. Orthop. Res.* **19**, 1021–1026 (2001).
8. L. Knott et al., "Biochemical changes in the collagenous matrix of osteoporotic avian bone," *Biochem. J.* **310**, 1045–1051 (1995).
9. A. J. Bailey et al., "Biochemical changes in the collagen of human osteoporotic bone matrix," *Connect. Tissue Res.* **29**(2), 119–132 (1993).
10. X. Banse, T. J. Sims, and A. J. Bailey, "Mechanical properties of adult vertebral cancellous bone: correlation with collagen intermolecular cross-links," *J. Bone Miner. Res.* **17**(9), 1621–1628 (2002).
11. A. J. Bailey et al., "Age-related changes in the biochemical properties of human cancellous bone collagen: relationship to bone strength," *Calcif. Tissue Int.* **65**, 203–210 (1999).
12. D. J. Leeming et al., "Is bone quality associated with collagen age?" *Osteoporosis Int.* **20**, 1461–1470 (2009).
13. C. F. Njeh, C. M. Boivin, and C. M. Langton, "The role of ultrasound in the assessment of osteoporosis: a review," *Osteoporosis Int.* **7**, 7–22 (1997).
14. P. Laugier, "Instrumentation for *in vivo* ultrasonic characterization of bone strength," *IEEE Trans. Ultrason. Ferroelect. Freq. Control* **55**(6), 1179–1196 (2008).
15. K. Mizuno et al., "Influence of cancellous bone microstructure on two ultrasonic wave propagations in bovine femur: an *in vitro* study," *J. Acoust. Soc. Am.* **128**(5), 3181–3189 (2010).
16. K. Yamashita et al., "Two-wave propagation imaging to evaluate the structure of cancellous bone," *IEEE Trans. Ultrason. Ferroelect. Freq. Control* **59**(6), 1160–1166 (2012).
17. K. Wear, "Ultrasonic scattering from cancellous bone: a review," *IEEE Trans. Ultrason. Ferroelectr. Freq. Control* **55**(7), 1432–1441 (2008).
18. K. W. Wear and B. S. Garra, "Assessment of bone density using ultrasonic backscatter," *Ultrasound Med. Biol.* **24**(5), 689–695 (1998).
19. F. Jenson, F. Padilla, and P. Laugier, "Prediction of frequency-dependent ultrasonic backscatter in cancellous bone using statistical weak scattering model," *Ultrasound Med. Biol.* **29**(3), 455–464 (2003).
20. M. A. Hakulinen et al., "Ultrasonic characterization of human trabecular bone microstructure," *Phys. Med. Biol.* **51**(6), 1633–1648 (2006).
21. O. Riekkinen et al., "Acoustic properties of trabecular bone relationships to tissue composition," *Ultrasound Med. Biol.* **33**(9), 1438–1444 (2007).
22. M. A. Hakulinen et al., "Ability of ultrasound backscattering to predict mechanical properties of bovine trabecular bone," *Ultrasound Med. Biol.* **30**(7), 919–927 (2004).
23. S. Chaffai et al., "Ultrasonic characterization of human cancellous bone using transmission and backscatter measurements relationships to density and microstructure," *Bone* **30**(1), 229–237 (2002).
24. B. K. Hoffmeister et al., "Ultrasonic characterization of human cancellous bone *in vitro* using three different apparent backscatter parameters in the frequency range 0.6–15 MHz," *IEEE Trans. Ultrason. Ferroelectr. Freq. Control* **55**(7), 1442–1452 (2008).
25. B. Hoffmeister, "Frequency dependence of apparent ultrasonic backscatter from human cancellous bone," *Phys. Med. Biol.* **56**, 667–683 (2011).
26. P. Laugier and G. Haïat, *Bone Quantitative Ultrasound*, Springer, Dordrecht, The Netherlands (2011).
27. F. Jenson et al., "*In vitro* ultrasonic characterization of human cancellous femoral bone using transmission and backscatter measurements relationships to bone mineral density," *J. Acoust. Soc. Am.* **119**(1), 654–663 (2006).
28. B. K. Hoffmeister et al., "Effect of collagen content and mineral content on the high-frequency ultrasonic properties of human cancellous bone," *Osteoporosis Int.* **13**, 26–32 (2002).
29. J. P. Karjalainen et al., "Ultrasound backscatter imaging provides frequency-dependent information on structure, composition and mechanical properties of human trabecular bone," *Ultrasound Med. Biol.* **35**(8), 1376–1384 (2009).
30. B. Lashkari and A. Mandelis, "Combined photoacoustic and ultrasonic diagnosis of early bone loss and density variations," *Proc. SPIE* **8207**, 82076K (2012).
31. B. Lashkari and A. Mandelis, "Coregistered photoacoustic and ultrasonic signatures of early bone density variations," *J. Biomed. Opt.* **19**(3), 036015 (2014).
32. L. Yang et al., "Bone composition: photoacoustics versus ultrasound," *Int. J. Thermophys.* (2014).
33. B. Lashkari, L. Yang, and A. Mandelis, "The application of backscattered ultrasound and photoacoustic signals for assessment of bone collagen and mineral contents," *Quant. Imaging Med. Surg.* **5**(1), 46–56 (2015).
34. G. Callis and D. Sterchi, "Decalcification of bone literature review and practical study of various decalcifying agents methods and their effect on bone histology," *J. Histotechnol.* **21**(1), 49–58 (1998).
35. H. Ehrlich et al., "Principles of demineralization modern strategies for the isolation of organic frameworks, part II decalcification," *Micron* **40**, 169–193 (2009).
36. C. Langton, "Osteoporosis: case of skeletal biocorrosion," *Corros. Eng. Sci. Technol.* **42**(4), 339–343 (2007).
37. B. Lashkari et al., "Slow and fast ultrasonic wave detection improvement in human trabecular bones using Golay code modulation," *J. Acoust. Soc. Am.* **132**(3), EL222 (2012).
38. B. Lashkari and A. Mandelis, "Linear frequency modulation photoacoustic radar: optimal bandwidth for frequency-domain imaging of turbid media," *J. Acoust. Soc. Am.* **130**(3), 1313–1324 (2011).
39. Panametrics, *NDT Ultrasonic Transducers for Nondestructive Testing*, Pana_UT_EN_201301, Olympus NDT (2011).
40. C. Gdyczynski et al., "On estimating the directionality distribution in pedicle trabecular bone from micro-CT images," *Physiol. Meas.* **35**, 2415–2428 (2014).
41. S. A. Goldstein, R. Goulet, and D. McCubbrey, "Measurement and significance of three-dimensional architecture to the mechanical integrity of trabecular bone," *Calcif. Tissue Int.* **53**(Suppl. 1), S127–S133 (1993).
42. K. Wear, "Fundamental precision limitation for measurements of frequency dependence of backscatter: application in tissue-mimiking phantoms and trabecular bone," *J. Acoust. Soc. Am.* **110**(6), 3275–3282 (2001).
43. X. Wang, D. L. Chamberland, and G. Xi, "Noninvasive reflection mode photoacoustic imaging through infant skull toward imaging of neonatal brains," *J. Neurosci. Methods* **168**, 412–421 (2008).
44. C. Huang et al., "Aberration correction for transcranial photoacoustic tomography of primates employing adjunct image data," *J. Biomed. Opt.* **17**(6), 066016 (2012).
45. O. Riekkinen et al., "Dual frequency ultrasound new pulse echo technique for bone densitometry," *Ultrasound Med. Biol.* **34**(10), 1703–1708 (2008).
46. J. Karjalainen et al., "Dual-frequency ultrasound technique minimizes errors induced by soft tissue in ultrasound bone densitometry," *Acta Radiol.* **49**, 1038–1041 (2008).

Lifeng Yang received his BS degree in physics from the University of Electronic Science and Technology of China (UESTC), Chengdu, China, in 2003. He received his MA degree in 2006 and PhD in 2012 in optical engineering from UESTC. Between February 2013 and February 2014, he was a visiting scholar in the Center for Advanced Diffusion-Wave Technologies (CADIFT), University of Toronto, Canada, for research in biomedical photoacoustic imaging.

Bahman Lashkari is a postdoctoral research associate at the CADIFT, University of Toronto, where he works on several photoacoustic and ultrasound projects. He received his PhD in the same lab working on frequency-domain photoacoustic imaging (2011). His research interests are in medical imaging and tissue characterization.

Joel W. Y. Tan is a senior undergraduate student in biomedical engineering at the University of Toronto. He is currently pursuing graduate studies in the field of medical imaging. His research interests include discovering novel techniques and applications in ultrasonic and photoacoustic imaging.

Andreas Mandelis is a full professor of mechanical and industrial engineering; electrical and computer engineering; and the Institute of Biomaterials and Biomedical Engineering, University of Toronto. He is the director of the CADIFT. He is the author and co-author of more than 330 scientific papers in refereed journals and 180 scientific and technical proceedings papers. He is an editor of the *Journal of Biomedical Optics*, *Journal of Applied Physics*, *International Journal of Thermophysics* and *Optics Letters*.